In and Out of Criticality? State-Dependent Scaling in the Rat Visual Cortex

Daniel M. Castro [1], Thaís Feliciano,[1] Nivaldo A. P. de Vasconcelos [2,3,4] Carina Soares-Cunha,[3,4] Bárbara Coimbra,[3,4] Ana João Rodrigues [3,4] Pedro V. Carelli [1] and Mauro Copelli [1,*]

[1]*Departamento de Física, Centro de Ciências Exatas e da Natureza, Universidade Federal de Pernambuco, Recife, PE, 50670-901, Brazil*
[2]*Departamento de Engenharia Biomédica, Centro de Tecnologia e Geociências, Universidade Federal de Pernambuco, Recife, PE, 50670-901, Brazil*
[3]*Life and Health Sciences Research Institute (ICVS), School of Medicine, University of Minho, 4710-057 Braga, Portugal*
[4]*ICVS/3B's - PT Government Associate Laboratory, 4805-017 Braga/Guimarães, Portugal*

The presumed proximity to a critical point is believed to endow the brain with scale-invariant statistics, which are thought to confer various functional advantages in terms of its information processing, storage, and transmission capabilities. To assess the relationship between scaling and cortical states, we apply a phenomenological renormalization group analysis to 3-h spiking data recordings from the urethane-anesthetized rat's visual cortex. Under this type of anesthesia, cortical states dynamically shift across a spectrum of synchronization levels, defined by population spiking rate variability. By developing a scaling criterion based on the kurtosis of the momentum-space activity distribution, our study combines the coarse-graining method with state-dependent analysis. We find that scaling signatures only appear as spiking variability surpasses a specified threshold. Notably, within this regime, scaling exponents show relative stability. Conversely, subthreshold activity is primarily asynchronous and fails to meet the scaling criterion. Our results suggest that a wide range of cortical states corresponds to small deviations around a critical point, with the system fluctuating in and out of criticality, spending roughly three-quarters of the experiment duration within a scaling regime.

I. INTRODUCTION

The concept of criticality in living systems has attracted growing interest in recent decades due to its potential to shed light on the behavior of complex biological systems, including the brain [1–6]. In particular, since the first observation of power-law-distributed neuronal avalanches in slices of the rat cortex by Beggs and Plenz [2], the critical brain hypothesis [4,5,7,8] has been intensively investigated both theoretically [9–26] and in diverse experimental setups [27–47].

Amongst the brain areas, the cerebral cortex has been the focal point in the exploration of the critical brain hypothesis, mainly the primary sensory cortices [2,4,34,43,48,49]. Such cortical areas play a paramount role in sensory processing from the environmental stimuli [50]. The technological development in simultaneous recordings of large neuronal populations [51] has fueled the exploration of the critical brain hypothesis at the neuronal population level, especially during periods in the absence of stimuli (spontaneous activity) [43,52]. The characteristics of this type of activity closely parallel those observed in spiking-evoked activity within the sensory cortex of freely moving animals, particularly in the

primary visual cortex (V1) [33,34,53,54]. Furthermore, spiking activity assumes different levels of variability in V1, with behavioral relevance [55]. The level of spiking variability has been used as a proxy for the cortical state [55–60].

Recently, Fontenele *et al.* proposed a relationship between criticality and cortical states in a study including spiking data of urethane-anesthetized rats [43]. In such experimental setup, cortical activity spontaneously drifts between more desynchronized states, similar to what one finds in awake and alert behavior, and more synchronized states, as observed in drowsiness and slow-wave sleep [55,61]. Spiking variability, characterized by the coefficient of variation (CV) of the population spiking rate, was chosen as a *de facto* control parameter to assess the cortical state every few seconds (with CV increasing with synchronization levels). Scaling relations of avalanche exponents were observed only for intermediate CV values, suggesting that a critical point occurred only in a narrow range of spiking variability, whereas the brain dynamics fluctuated widely around this point. In other words, the brain would be close to criticality frequently, but still *en passant*. Very often it would operate with ranges of spiking variability that did not satisfy scaling relations of avalanche exponents [43].

This interpretation was later challenged by Carvalho *et al.* [24], who reproduced most of the experimental results with an analytically solvable model. The model has a true control parameter, which accounts for the relative weight of inhibitory coupling [62]. By changing this control parameter within only 3% of its critical value, the model could reproduce almost the whole range of spiking variability observed in the data. These

*mauro.copelli@ufpe.br

results therefore suggest that CV, as employed by Fontenele *et al.* [43], is actually not a good "effective" control parameter after all, since it fluctuated widely even for a fixed value of the *bona fide* control parameter of the model. Moreover, they raised the possibility that the urethanized rat cortex was actually close to the critical point most of the time, instead of only *en passant*. The model identifies subsampling in spiking data as the key ingredient responsible for distorting avalanche results, causing them to inaccurately suggest that the system is not critical, when in fact it is [24].

If true, these results suggest that too large and too small values of spiking variability would correspond to small fluctuations around the critical point, a possibility that would be important for the understanding of cortical states. Yet, these inferences rely exclusively on model-derived results. How can we go about testing whether this is true in the real data?

What we propose here is to address this question by analyzing the data with the phenomenological renormalization group method (PRG) introduced by Meshulam *et al.* [63]. The method consists of gradually coarse-graining neuronal data, much like Kadanoff's renormalization group block spins method [64]. The renormalization group intuition is that, given a system's scale invariance at a second-order phase transition, its collective dynamics is not sensitive to most microscopic details. Thus, the recursive coarse-graining procedure should lead to a fixed point in model space. This, in turn, is reflected in nontrivial scaling exponents associated with different statistical features, as well as non-Gaussian activity distribution. The PRG method conforms to these ideas by yielding scaling exponents without relying on an explicit model.

To assess to which extent scaling persists as spiking variability changes, we conjugate the PRG method [63] with a state-dependent analysis, segmenting the data by CV [43]. If indeed the brain is deviating significantly from criticality as CV values fluctuate to very large or very small values, the scaling exponents as revealed by the PRG should be trivial in these extremes. But are they?

II. METHODS

A. Data acquisition and preprocessing

Nine extracellular recordings of ongoing activity in the rat's primary visual cortex (V1) under urethane anesthesia are used. Each recording is about 3 h long. All nine datasets use the same surgery and recording protocol, as previously described [24,43,65].

As described previously, the recording has been done from nonalbino and albino urethane-anesthetized male 3- to 4-month-old rats (Long-Evans, $n = 2$ [24]; Wistar-Han, $n = 7$ [65]). They were anesthetized with urethane (1.58 and 1.44 g/kg, respectively). As soon as the animal reached plane anesthetics, the surgery including trichotomy, craniotomy, and durotomy (only nonalbino) was performed. The coordinates used to guarantee V1 recording access [66] were AP (anteroposterior) $= -7.2$ mm and ML (mesolateral) $= 3.5$ mm.

A 64-channel silicon probe (BuzsakiA64sp, Neuronexus) with six shanks 200 μm apart was implanted in the primary visual cortex deep layers. In each shank, ten channels of area

160 μm² were disposed from the shank tip in a staggered configuration, 20 μm apart. Four extra channels exist along the fourth shank for tissue depth reference. The raw data were sampled at 30 kHz (16 bits/sample), amplified, and digitized in a single head-stage Intan RHD2164. The extracellular electric potential raw data was preanalyzed using Klusta-Team Software.

Out of the nine recordings, seven were performed at the University of Minho/School of Medicine abiding by the European regulations (European Union Directive 2010/63/EU), and all the experiments were approved by the Ethics Committee of the University of Minho (SECVS protocol #107/2015). Two of the recordings were performed at the Systems and Computational Neuroscience Laboratory at the Federal University of Pernambuco in strict accordance with the CONCEA-MCTI directives and were approved by the Federal University of Pernambuco (UFPE) Committee for Ethics in Animal Experimentation (23076.030111/2013-95 and 12/2015).

We employed both single-unit and multiunit activities (SUA and MUA). Data were divided in 50-ms bins, as previously described [43–45]. A unit i was considered active [$\sigma_i(t) = 1$] if there was a least one spike within a bin centered at time t, and inactive [$\sigma_i(t) = 0$] otherwise. The population firing rate $\rho(t)$ at each bin was estimated as the total number of spikes divided by the bin duration. Due to the nature of the method, only experiments with $N \geqslant 256$ units were selected for this analysis.

B. The PRG procedure

In this subsection, we provide a brief overview of the PRG coarse-graining procedure, which is described in detail in previous works [63,67]. In the context of the usual renormalization group applied to, say, the Ising model, Kadanoff's original idea of grouping neighboring spins into blocks makes sense because the interactions are known and local. Since the interactions are typically unknown for neuronal data, the idea of the PRG method is to make use of pairwise correlations as a proxy.

The procedure consists of repeatedly grouping the most correlated pair of neurons until there are no other pairs left. If $\sigma_i^{(1)}(t)$ is the binary ($\sigma_i^{(1)} \in \{0, 1\}$) time series of neuron i ($i = 1, \ldots, N$), then after the first PRG iteration one has $N/2$ coarse-grained variables, or "clusters":

$$\sigma_i^{(2)} = \sigma_i^{(1)} + \sigma_{j_*(i)}^{(1)}, \tag{1}$$

where $\sigma_{j_*(i)}^{(1)}$ is the neuron maximally correlated with $\sigma_i^{(1)}$. After k such iterations, we have $N_C = N/2^k$ units (clusters) $\{\sigma_j^{(k+1)}\}_{j=1,\ldots,N_C}$, each of size $C_{\text{size}} = 2^k$ (Fig. 1). To ensure we restrict our analysis to cases where enough iterations can be made, data trials with $N < 256$ are excluded.

Under this scheme, the presence of a nontrivial fixed point in the renormalization group should be assessed by scaling relations on several statistical quantities, namely, the mean variance, the silence probability, the covariance matrix spectrum, and the mean autocorrelation characteristic time. Additionally, the activity distribution under a nontrivial fixed point should approach a non-Gaussian form [63].
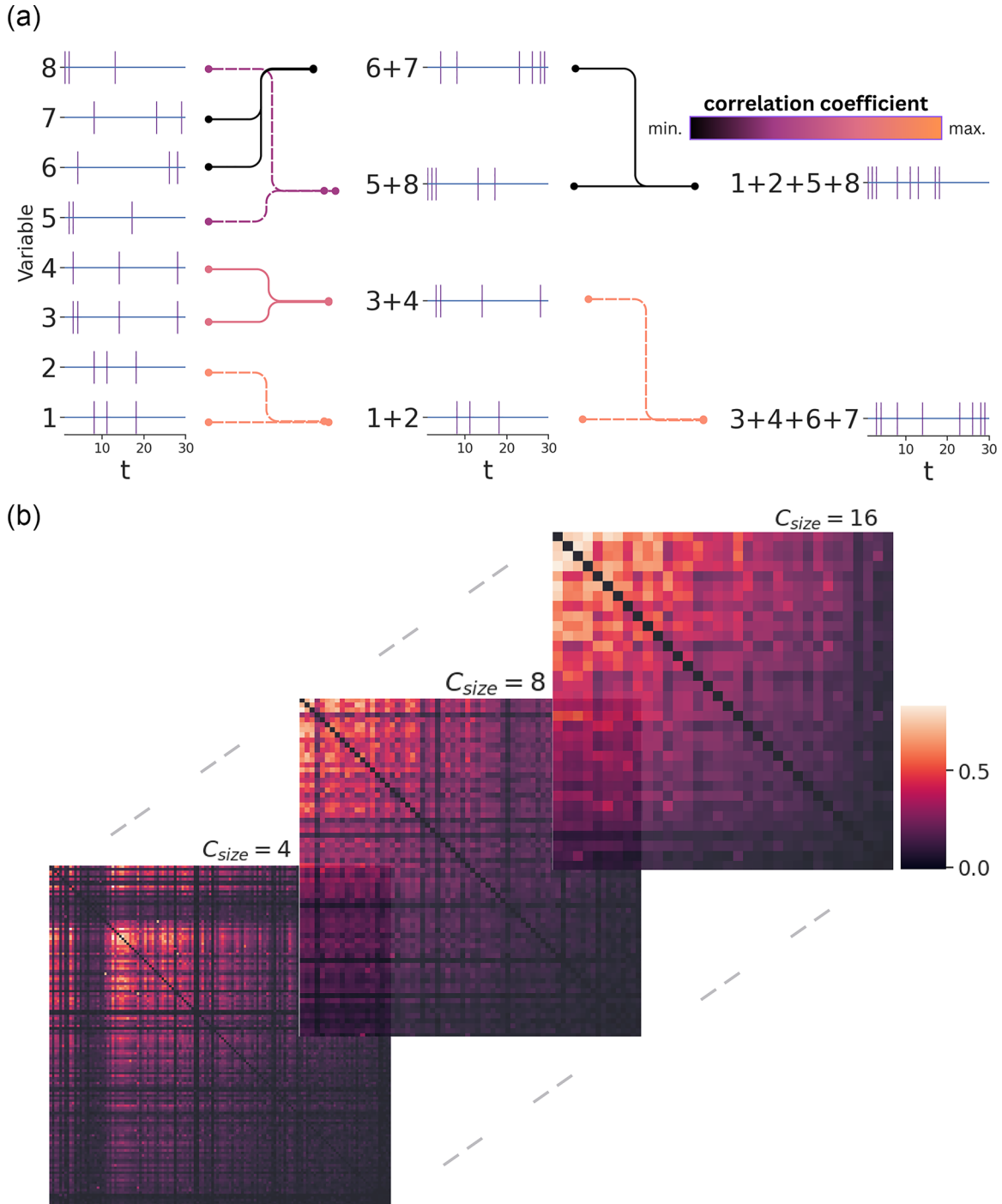
FIG. 1. (a) Visual scheme for the PRG procedure. Repeated iterations sum up maximally correlated variables, resulting in clusters of size $C_{\text{size}} = 2^k$ after k iterations. (b) Data subject to the coarse-graining procedure. Correlation matrices for $C_{\text{size}} = 4$, 8, and 16 provide us a visualization of the change of scale after each step. Diagonal terms were removed for visualization purposes.

1. Mean variance

The mean variance of the activity of clusters of size C_{size} is written as

$$M_2(C_{\text{size}}) = \frac{1}{N_C} \sum_{i=1}^{N_C} \left[\left\langle \left(\sigma_i^{(k+1)} \right)^2 \right\rangle - \left\langle \sigma_i^{(k+1)} \right\rangle^2 \right]. \quad (2)$$

Here, angle brackets denote temporal averages. M_2 grows with cluster size as

$$M_2(C_{\text{size}}) \propto C_{\text{size}}^{\tilde{\alpha}}, \quad (3)$$

where one expects $\tilde{\alpha} = 1$ for independent variables and $\tilde{\alpha} = 2$ for completely correlated ones. Nontrivial self-similar structure should present itself as an intermediate exponent between those two values.

2. Probability of silence

When examining the distribution of individual coarse-grained variables, we can track the probability that a cluster remains silent at a given moment. For independent variables, such probability decays exponentially, as clusters are simply sums of uncorrelated activity. The presence of self-similarity is assessed again through a power-law:

$$\mathcal{F}(C_{\text{size}}) \equiv -\log \mathcal{P}_{\text{silence}} \propto C_{\text{size}}^{\tilde{\beta}}. \quad (4)$$

$\mathcal{F}(C_{\text{size}})$ can be thought of as an effective free energy of the system [63], although there is no definition for a temperature in this case. For independent variables, one expects, therefore, $\tilde{\beta} = 1$. As the summing of identical variables does not affect $\mathcal{P}_{\text{silence}}$, the perfectly correlated case gives the opposite boundary $\tilde{\beta} = 0$.

3. Characteristic autocorrelation time

A third scaling relation results from dynamical scaling of the coarse-grained variables. From the autocorrelation function of an individual cluster, namely,

$$C_i(C_{\text{size}}, t) = \frac{\left\langle \left(\sigma_i^{(k+1)}(t_0) \sigma_i^{(k+1)}(t_0+t) \right) - \left\langle \sigma_i^{(k+1)} \right\rangle^2 \right\rangle}{\left\langle \left(\sigma_i^{(k+1)} \right)^2 \right\rangle - \left\langle \sigma_i^{(k+1)} \right\rangle^2}, \quad (5)$$

we take the average across all clusters

$$C(C_{\text{size}}, t) = \frac{1}{N_C} \sum_i^{N_C} C_i(C_{\text{size}}, t). \quad (6)$$

From here, we can define the characteristic autocorrelation time as $C(C_{\text{size}}, \tau_c) = 1/e$. In the presence of dynamical scaling, it should behave as $\tau_c \propto C_{\text{size}}^{\tilde{z}}$. For uncorrelated units, we find trivial exponential decay at all iterations ($\tilde{z} = 0$).

4. Covariance spectrum

We start with the intracluster covariance matrix, defined by

$$C_{ij} = \left\langle \sigma_i^{(1)} \sigma_j^{(1)} \right\rangle - \left\langle \sigma_i^{(1)} \right\rangle \left\langle \sigma_j^{(1)} \right\rangle, \quad (7)$$

with $\sigma_i^{(1)}$ and $\sigma_j^{(1)}$ being all original variables belonging to a cluster at the kth iteration $\sigma^{(k+1)}$. From this matrix, we take its eigenvalues $\{\lambda_r\}_{r=1,\dots,C_{size}}$, defined by

$$\sum_r^{C_{\text{size}}} C_{ij} u_{jr} = \lambda_r u_{ir}, \quad (8)$$

and rank them in descending order. The resulting curve has also been shown [63] to have scaling relations at a renormalization group fixed point:

$$\lambda_r \propto \left(\frac{C_{\text{size}}}{r} \right)^\mu. \quad (9)$$

Notice that scaling occurs concomitantly with shape collapse of the eigenvalues decay, another signature of scale invariance.

5. Momentum space activity distribution and its kurtosis

When analyzing the activity distribution of coarse-grained variables, we make use of a momentum space (MS) transformation [68]. This is done by employing a subset of the covariance matrix eigenvectors $\{\mathbf{u}_r\}$, in descending order of their respective eigenvalues, by means of the projectors

$$\hat{P}_{ij}(N_{\text{modes}}) = \sum_{r=1}^{N_{\text{modes}}} u_{ir} u_{jr}, \quad (10)$$

where $N_{\text{modes}} = N, N/2, \dots, N/2^k$. With these projectors we can build momentum space coarse-grained variables,

$$\phi_i(N_{\text{modes}}) = z_i(N_{\text{modes}}) \sum_j^N \hat{P}_{ij}(N_{\text{modes}})\left[\sigma_j^{(1)} - \left\langle \sigma_j^{(1)} \right\rangle \right], \quad (11)$$

where $z_i(N_{\text{modes}})$ is chosen to make $\langle \phi_i^2(N_{\text{modes}}) \rangle = 1$ [67]. In this case, coarse-graining amounts to including an ever smaller fraction of modes into building the new variables. This can be done because, for systems with translational invariance, the eigenvalue spectrum is equivalent to the Fourier transform of the correlation matrix [67]. In particular, we are interested in the activity distribution of the coarse-grained variables:

$$P_{N_{\text{modes}}}(\phi) = \frac{1}{N} \sum_{i=1}^N \mathbb{P}[\phi_i(N_{\text{modes}}) = \phi]. \quad (12)$$

In this representation, a trivial distribution (i.e., without strong enough correlations) would fall into a Gaussian form for a sufficiently small number of modes, whereas self-similarity presents itself as a non-Gaussian distribution. To assess the Gaussianity of the distribution, we calculate the kurtosis $\kappa = \langle \phi^4 \rangle / \langle \phi^2 \rangle^2$. For a Gaussian distribution, $\kappa = 3$.

C. Surrogate data and scaling criterion

In order to test the robustness of our results, we repeat all the procedures for surrogate data, which were obtained by shuffling the interspike intervals of each unit within each analyzed time window (see Sec. II D).

We also choose a criterion to explicitly determine the presence or absence of scaling in our data based on surrogate data. For each analyzed time window, we compare the kurtosis of the corresponding MS activity distribution [Eq. (12)] with the kurtoses of the distributions of MS surrogate data of all windows from the time series. Note that this is a stronger criterion than comparing with the kurtosis of a single window. We consider the activity in the time windows to present scaling if the value of its kurtosis is 1 standard deviation above the mean kurtosis of the surrogate data.

D. State-dependent analysis

To assess how different levels of spiking variability may impact the coarse-graining analysis, we segment our data into 30-s windows. For the jth such window, we extract the population firing rate coefficient of variation (CV), defined as

$$\text{CV}_j = \frac{\sqrt{\langle \rho^2 \rangle_j - \langle \rho \rangle_j^2}}{\langle \rho \rangle_j}, \quad (13)$$

where $\rho(t)$ is the "instantaneous" firing rate (estimated every 50-ms time bin) and averages are taken within the jth time
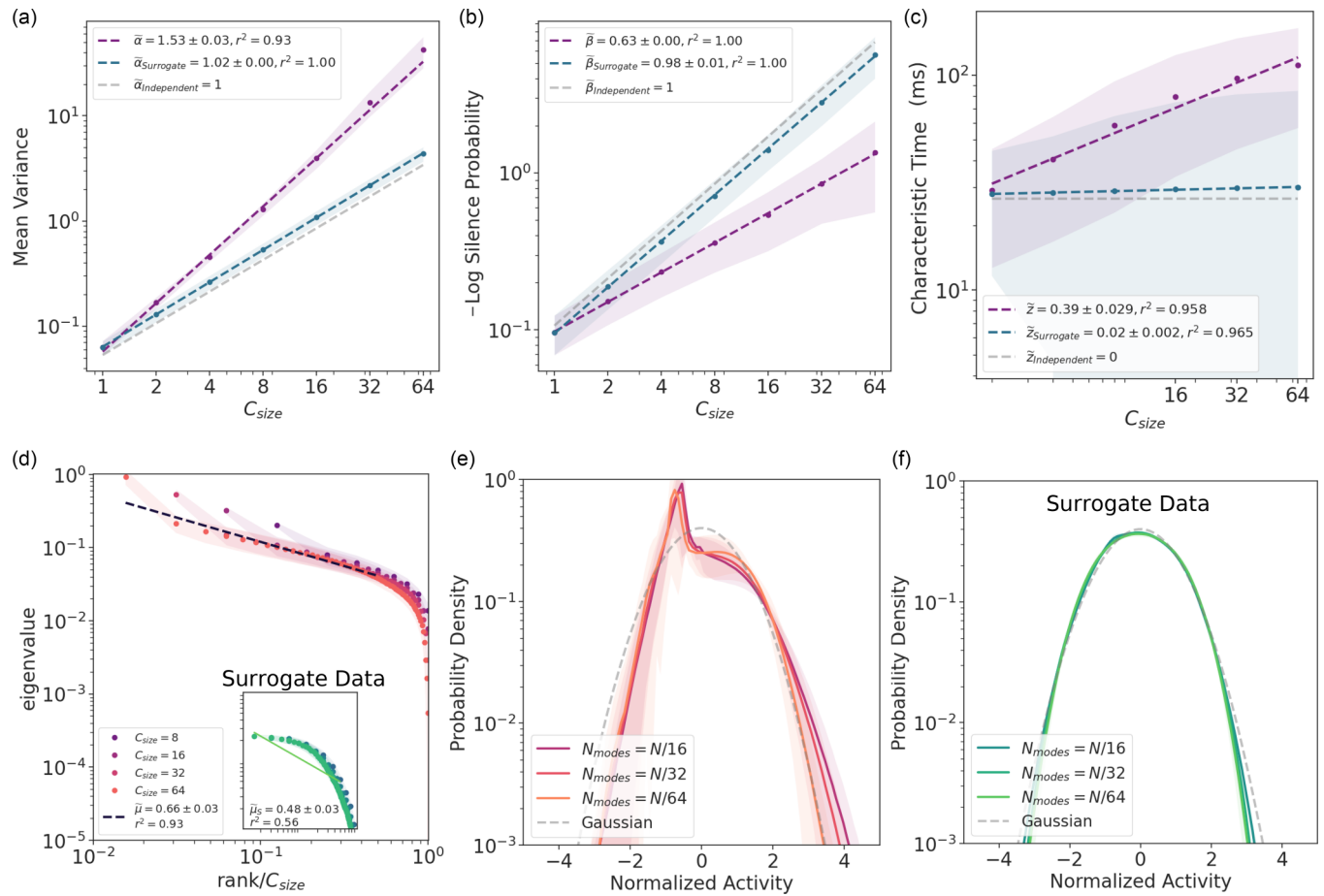
FIG. 2. Scaling relations obtained from the coarse-graining procedure for a single animal. (a) Mean variance, (b) silence probability, and (c) characteristic autocorrelation decay time as functions of cluster size. (d) Intracluster spectrum of the covariance matrix. Panels (e) and (f) show the probability density $P_K(\phi)$ of MS coarse-grained variables in the original and surrogate data, respectively. In panels (a)–(d), r^2 stands for the usual coefficient of determination, used to assess the quality of our power-law fits. Points (shades) are averages (standard deviations) across all the 600-s windows.

window. We note that CV as defined above is also referred to as "population firing rate variability" [69], but here we refer to it as "spiking variability" for simplicity.

As mentioned previously, CV can be used as a proxy for the cortical state, with higher (lower) values corresponding to more (less) synchronized spiking activity. Accordingly, pairwise correlations increase monotonically with increasing CV [24,43,65].

We parse windows according to their CV values and investigate how scaling relations are affected by different levels of spiking variability, i.e., across the spectrum of cortical states. We then group results and average across windows of similar CV values.

III. RESULTS

A. State-independent scaling results

Initially, we investigate the outcomes of applying the PRG procedure to raw spiking data. In other words, at first we disregard the fact that the spiking variability changes a lot in the scale of the whole experiment and we obtain results regardless of the CV value. The PRG procedure is applied to

600-s windows of the whole time series and then averaged across those windows.

We find that, for each animal, the mean variance of the cluster activity increases with cluster size as a power law with a nontrivial exponent $1 < \alpha < 2$ [Eq. (3) and Fig. 2(a)]. For surrogate data, obtained by shuffling the interspike intervals of each neuron within a given time window, results are closer to what is expected for independent data.

As we progressively coarse grain and our variables become sums of an increasing number of neurons, the probability of a variable being completely silent decreases for large C_{size}. We obtain a power-law decay for the free energy with $\widetilde{\beta} < 1$, as expected for self-similar correlations [Eq. (4) and Fig. 2(b)]. Surrogate data, on the other hand, show a faster decay, which amounts to the trivial case $\widetilde{\beta} = 1$.

Dynamical scaling can also be found in the coarse-grained variables. With autocorrelation decaying exponentially with characteristic time τ_c, we find that $\tau_c \propto C_{\text{size}}^{\widetilde{z}}$ [Fig. 2(c)]. This means that, as we look at clusters comprising an increasing number of neurons, their autocorrelation takes longer to decay. For surrogate data, this correlation time is independent of cluster size.
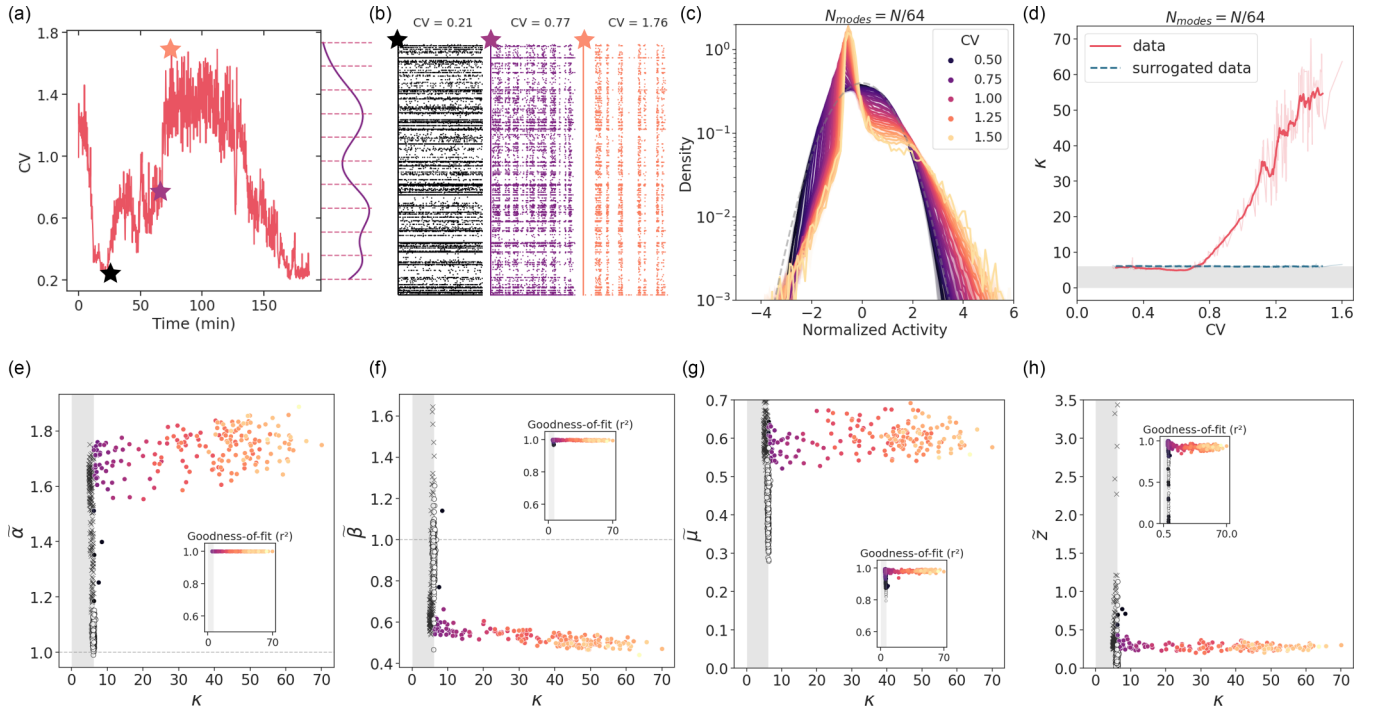
FIG. 3. Results of state-dependent PRG analysis for the same subject shown in Fig. 2. (a) Example of the coefficient of variation over time for a single experiment. The curve on the right depicts a histogram of CV. (b) Examples of raster plots for different CV values. (c) Activity distribution of variables built from $N/64$ eigenmodes. Each curve averages all trials within a range of CV [in this case separated in 30 quantiles, 3 between each dashed line in (a)]. (d) Kurtosis of the distribution of MS coarse-grained variables (built from $N/64$ eigenmodes). The darker curve is the moving average over windows of 12 consecutive points. Gray stripes comprise the range of κ values that fail to meet the scaling criterion (Sec. II C), i.e., $0 \leqslant K \leqslant \langle K \rangle^{\mathrm{surrogate}} + \sigma_K^{\mathrm{surrogate}}$. (e)–(h) Impacts of state dependence on the scaling exponents. (e), (f) Exponents for the scalings of the mean variance ($\widetilde{\alpha}$) and log silence probability inside a cluster ($\widetilde{\beta}$). For low enough CV, such that κ is within the surrogate range, exponents (represented by crosses) approach their trivial values of 1, close to the surrogate results (white dots). Increasing CV, exponents continuously evolve to a stable value. (g), (h) Exponent $\widetilde{\mu}$ for the scaling of the covariance matrix eigenvalues and exponent $\widetilde{z}$ for the scaling of the mean autocorrelation decay time. In these cases, state-dependent analysis does not directly impact the scaling exponents' values, although exponents obtained from low CV trials, like surrogate data, fail to achieve a good power-law fit.

The last power-law relationship comes from the eigenvalue spectrum of the covariance matrix. We find that the eigenvalues decay with rank with an exponent $\widetilde{\mu} < 1$ [Eq. (9)], but not so for the surrogate data [Fig. 2(d)].

Finally, we also obtain the probability distribution of the activity as we coarse-grain variables by reducing the number of modes in momentum space (Sec. II B 5). The procedure leads to a non-Gaussian distribution [Fig. 2(e)], which is a signature of a self-similar correlation structure. Surrogate data, on the other hand, are consistent with a trivial Gaussian distribution [Fig. 2(f)].

Averaging these results over the group of nine animals [henceforth denoted by $\langle \cdots \rangle_g$], we obtain $\langle \widetilde{\alpha} \rangle_g = 1.66 \pm 0.28$, $\langle \widetilde{\beta} \rangle_g = 0.70 \pm 0.08$, $\langle \widetilde{z} \rangle_g = 0.33 \pm 0.07$, and $\langle \widetilde{\mu} \rangle_g = 0.56 \pm 0.10$. To quantify the difference between the activity distributions of regular and surrogate data, we obtain the following values of kurtosis at the highest level of coarse graining: $\langle \kappa \rangle_g = 43 \pm 23$ and $\langle \kappa \rangle_g^{\mathrm{surrogate}} = 6.4 \pm 1.4$. As we see in the following, the large standard deviation observed in the kurtosis of the actual data is a consequence of having disregarded the wide variation of cortical states produced by urethane [24,43,61,65]. This amounts to lumping together regimes which, as far as scaling is concerned, turn out to be quantitatively and qualitatively different.

B. State-dependent scaling results

Next, we investigate to which extent the scaling results change as we parse the data according to spiking variability. The procedure is similar to that of previous studies [24,43,44,65], as we calculate the CV of the population firing rate in windows of 30 s and run the PRG analysis pipeline in each window (Sec. II D).

The cortical CV time series of a typical urethane-anesthetized rat is erratic [Fig. 3(a)], with low values corresponding to asynchronous activity and high values corresponding to more synchronized spiking [Fig. 3(b)]. Low and high levels of CV and synchronization, on the other hand, are associated with low and high mean values of pairwise spiking correlations [55]. Given that these correlations play an essential role in the PRG coarse-graining procedure, it is reasonable to expect that CV levels will have some impact on the results.

And, indeed they do. When the MS coarse-graining is applied to high-CV data, the procedure converges to nontrivial (i.e., non-Gaussian) activity distributions [Fig. 3(c)]. However, as the value of CV under analysis is gradually decreased, the distributions eventually approaches a trivial, Gaussian-like shape [Fig. 3(c)].
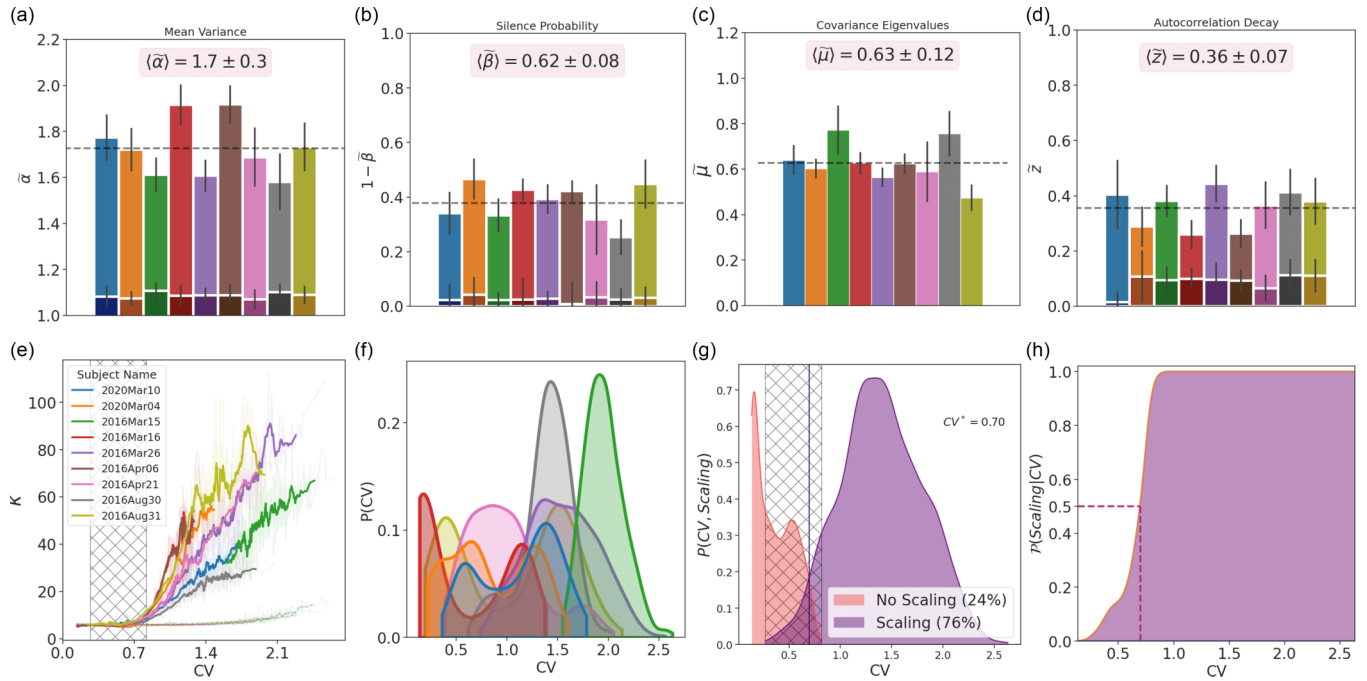
FIG. 4. (a)–(d) Averages (bars) and standard deviation (vertical lines) of state-dependent scaling exponents of each subject (darker shades with white contour represent surrogate results). Bars for the $\widetilde{\mu}$ exponent from surrogate data are not shown, as its covariance spectrum is not well adjusted by a power law [see inset of Fig. 2(d)]. Dashed horizontal lines are group averages. (e) Kurtosis as a function of CV for each subject. Results for real (surrogate) data in solid (dashed) lines. Hatched area represents the region where both scaling and no scaling may be found for a given subject [also depicted in panel (g) for the group average]. (f) $P(\text{CV})$ for each subject. (g) $P(\text{CV}, \text{scaling})$: Probability densities of CV for trials that do or do not exhibit scaling. Hatched area covers the range of CV where both scaling and no scaling may be found, and a vertical line at $\text{CV}^* = 0.70$ marks the point at which scaling and no scaling are equiprobable. (h) $P(\text{scaling}|\text{CV})$: Conditional probability density of finding scaling given a CV value.

Employing the kurtosis to assess the non-Gaussianity of the distributions, we observe that its dependence on spiking variability is remarkable: for low enough CV, the distributions are comparable to the Gaussians observed in surrogate data [Fig. 3(d)]; above a characteristic value of CV ($\simeq 0.7$), the kurtosis departs from its surrogate value and then increases monotonically [Fig. 3(d)]. The MS coarse-graining analysis therefore suggests two qualitatively different regimes, a trivial one below a characteristic CV value and a nontrivial one above it.

The dependence of kurtosis on spiking variability is similar to a typical plot of order parameter versus control parameter in a second-order phase transition, but such a comparison, almost irresistible at first glance, would be wrong. The excess kurtosis in the urethane data is a signature of nontrivial scaling at *all points* above a certain level of CV. This is in contrast to the scaling expected at a single critical value of the control parameter in a phase transition [70]. The results of the PRG coarse-graining procedure therefore support the conjecture put forward by Carvalho *et al.* [24] that CV indeed is not a good candidate for a control parameter.

The behavior of the other exponents aligns consistently with this interpretation. Employing kurtosis above surrogate levels as a criterion for proper scaling (as detailed in Sec. II C), we find again two qualitatively distinct behaviors. For low CV ($\lesssim 0.7$) and near-surrogate κ, scaling relations exhibit poor goodness-of-fit, resulting in exponents that span a wide range of values [as indicated by the gray regions in Figs. 3(e)–3(h)].

However, as CV increases sufficiently ($\gtrsim 0.7$), causing κ to depart from its surrogate levels and reveal the non-Gaussian nature of the activity distributions, the exponents $\widetilde{\alpha}$, $\widetilde{\beta}$, $\widetilde{\mu}$, and $\widetilde{z}$ stabilize within scaling relations characterized by excellent goodness-of-fit [Figs. 3(e)–3(h)]. Note that these stable values differ slightly from the values obtained for the state-independent analysis (shown in Sect. III A), since those mix together two regimes that in hindsight we discover to be completely different.

C. Group results

We systematically repeat the state-dependent scaling analyses for all nine subjects available in our study. By computing averages over data segments that meet our defined scaling criterion (Sec. II C), we observe a consistent behavior of exponents across the subjects ($\widetilde{\alpha} = 1.7 \pm 0.3$, $\widetilde{\beta} = 0.62 \pm 0.08$, $\widetilde{\mu} = 0.63 \pm 0.12$, and $\widetilde{z} = 0.36 \pm 0.07$), and the range of these exponents exclude their surrogate counterparts [Figs. 4(a)–4(d)].

Although the range of kurtosis values varies across subjects [Fig. 4(e)], this variation is in line with their widely different distributions of spiking variability [Fig. 4(f)]. Notably, despite these differences, the characteristic CV value at which scaling emerges remains remarkably robust [Fig. 4(e)].

It is important to note that, below the characteristic CV value, fluctuations in the kurtosis allow it to enter and leave the region that we chose to be our scaling criterion [gray

stripe in Fig. 3(d)]. We therefore estimate the joint probability P(scaling, CV) (see Supplemental Material [71]), which skews towards higher CV values in the presence of scaling and lower CV values in its absence [Fig. 4(g)]. Overall, we observe that a substantial proportion of the subjects' data analysis time is spent within the scaling regime, accounting for 76% of the entire duration [Fig. 4(g)]. Still, the nonscaling regime is far from negligible. These metrics can also be calculated for each subject (Figs. S2–S10 in the Supplemental Material [71]) and then averaged, yielding 72% ± 21% of the time spent within the scaling regime.

Alternatively, we also calculate the conditional probability P(scaling|CV) which, for the group data, reveals a characteristic CV value at half-height of 0.7 [Fig. 4(h)]. This parameter can be estimated for each subject and then averaged, resulting in a group-average of $\langle CV \rangle_g = 0.72 \pm 0.06$ (see Supplemental Material [71] for more details).

IV. CONCLUDING REMARKS

We have applied the coarse-graining procedure proposed by Meshulam *et al.* [63] to spiking data from the primary visual cortex of urethane-anesthetized rats and shown that it consistently yields signatures of scale invariance. Then we investigated to which extent these results depended on spiking variability, which is a proxy for cortical states. The association between cortical states and behavior is well established, with asynchronous states appearing during active waking and REM sleep, for instance, and synchronous states appearing during drowsiness and slow-wave sleep [55]. Urethane anesthesia is a convenient experimental setup that allows us to explore a wide range of cortical states, from asynchronous to synchronous regimes, and probe whether there is any relationship between these regimes and scaling.

To determine the presence of scaling in a given time window, we compared the kurtoses of the MS activity distribution and of the surrogate data. As we analyzed data with increasing values of spiking variability, the scaling criterion was met only above a characteristic value of CV, and exponents gradually flowed from trivial values to nontrivial ones. Moreover, in the presence of nontrivial scaling, exponents were relatively stable. If we interpret scaling as a sufficient signature of a second-order phase transition, our results suggest that the system goes in and out of criticality, spending on average about three quarters of the experiment duration in a scaling regime.

Interestingly, the CV time evolution differs completely among the nine analyzed rats. Nonetheless, all of them cross the threshold between scaling and no scaling in the same CV range. This means that, to some extent, we can infer the existence of scale-invariant dynamics within a given time window based solely on its spiking variability.

These findings are in stark contrast with what has been obtained via avalanche analysis in the same dataset [43]. That difference is central to the significance of our results. Fontenele *et al.* obtained scaling of avalanche exponents only within a narrow range of intermediate CV values, which was interpreted as a critical point with CV playing the role of a control parameter of the system [43]. Carvalho *et al.* [24], on the other hand, showed that a model with a well-defined order parameter tuned very close to criticality could reproduce the whole range of experimentally observed CVs, therefore suggesting that CV would be a poor control parameter. Additionally, it suggested that avalanche-based results were distorted by subsampling effects, yielding signatures of noncriticality for a system that was, in fact, critical [24]. The application of the phenomenological renormalization group to urethane data presented here supports the model results of Carvalho *et al.* [24]: the PRG signatures of criticality are present in the same broad range of CV values that had been predicted by the model.

One aspect currently overlooked by the PRG approach is the influence of varying temporal resolutions on the outcomes of the method. The selection of time bin durations to define statistical events, particularly when assessing criticality in experimental data, remains a persistent challenge in the field. Depending on the dataset, a wide range of timescales have been employed to bin the data in different approaches to assess criticality [72–76]. In our analyses, we opted to standardize bin duration to 50 ms to ensure consistency with our primary sources for result comparison [24,43]. However, recognizing the importance of exploring temporal scales, we conducted additional analyses on a single subject's data to investigate how different temporal resolutions might alter previously obtained results. Unsurprisingly, we find that PRG scaling exponents are sensitive to the choice of bin duration (see Supplemental Fig. S1 [71]), as it is known to occur with previous methods used to empirically measure scale invariance [24,42].

In recent years, a rich debate has flourished on whether the nontrivial, scale-free statistics found in brain activity stems from type-1 criticality (scale-invariant avalanches [2]), type-2 criticality (edge-of-chaos [77]), or a combination of these, not mutually exclusive in principle [78]. Since in our case only a small fraction of the cortex is being measured, there is even another possibility involving multiple external drivings, which can also result in scale-invariant statistics [79]. Regardless of the cause, the intermittency of self-similarity in cortical dynamics invites us to think of which mechanisms could explain this phenomenon. It might be, for instance, a signature of self-organized quasicriticality, as proposed in a family of models with homeostatic dynamics [17,18,21,22,62,80–82].

Spiking data from nonanesthetized animals has recently been examined within the PRG framework [75]. A logical progression from this analysis could be applying the state-dependent approach outlined in this study to similar datasets. This would allow one to check to which extent the results obtained here for cortical states visited by the urethane-anesthetized cortex can be extended to cortical states that occur under more natural conditions. The fact that asynchronous states in nonanesthetized animals do show signatures of critical behavior [75], whereas under urethane they do not, suggests that not all asynchronous states are equivalent. On one hand, this should not be surprising, given the obvious behavioral differences between the two conditions. On the other hand, it underscores the necessity of developing new tools to characterize asynchronous states electrophysiologically, since both awake and urethanized cortices display similar CV values and pairwise correlation structures [43,55].

Given the model-independent nature of the phenomenological renormalization group technique, its applicability extends to any high-dimensional data amenable to binarization. Subsequent studies could explore the presence of scaling across various experimental setups and within novel systems. Adapting its usage to human data, as has been done recently [83], could provide us with markers for clinical aspects of analyzed subjects, for example. This advancement would not only broaden the utility of scaling analyses beyond theoretical realms but also render them more accessible and appealing to a broader audience, potentially sparking greater interest in the subject.

ACKNOWLEDGMENTS

APPENDIX: SUA AND MUA

The fact that we employ both SUA and MUA might lead to the concern that mixing together these different types of activity will lead to distortions under the PRG procedure. For instance, one MUA might contain spikes from multiple neurons, hence murking the definition of a "cluster size." Moreover, MUAs typically have higher firing rates than SUAs; hence, one could expect that the PRG procedure would have a bias to favor the clustering of MUAs together, therefore resulting in some clusters that represent far more actual neurons than other clusters.

We probe these issues by calculating the fraction of actual MUA + MUA, SUA + SUA, and SUA + MUA pairs in the first step of the PRG procedure (across all 30 s time windows) and comparing these fractions with what would be obtained by randomly pairing the MUAs and SUAs. For instance, if we have s SUAs and m MUAs in a given dataset, then the total number of *possible* pairs is $T = \binom{s+m}{2}$. The fractions of MUA + MUA, SUA + SUA and SUA + MUA *possible* pairs are respectively $\binom{m}{2}/T$, $\binom{s}{2}/T$, and sm/T. If there were a problem with a bias in the PRG procedure, then we would expect
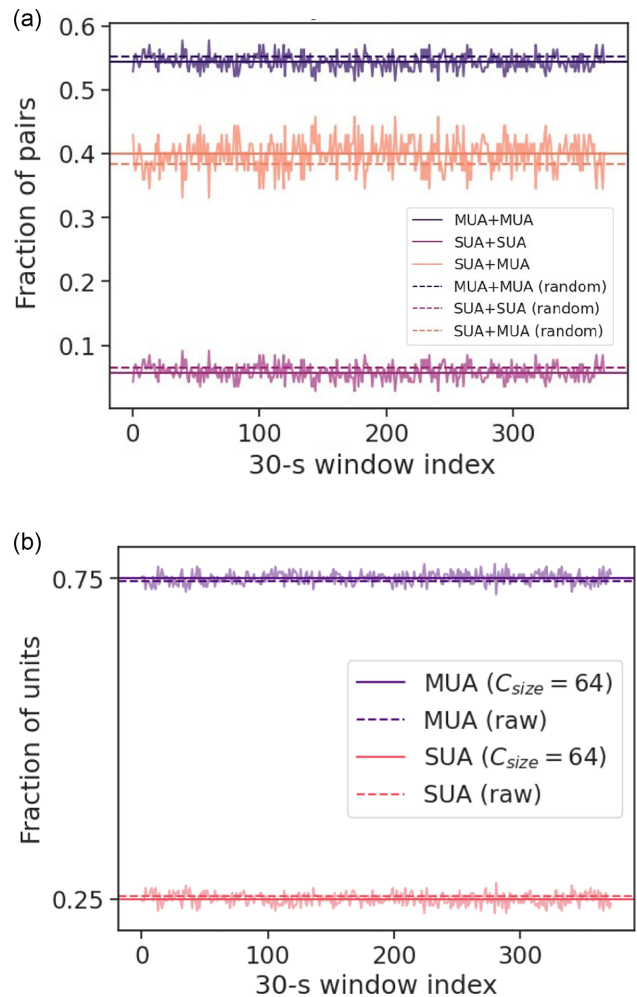
FIG. 5. Comparison of how MUAs and SUAs are joined together by the PRG procedure. (a) For each 30-s time window analyzed, we calculate the ratio of MUA + MUA, SUA + MUA, and SUA + SUA pairs in the first PRG iteration. Then, we compare their averages (solid straight lines) with the ratio expected from random pairings (dashed lines). We can see that the PRG does not favor combining MUAs with themselves. In panel (b), we examine the final iteration of the PRG, calculating the fractions of MUAs and SUAs within each cluster (solid lines). The ratios are similar to those of the raw variables (dashed lines).

to observe a much larger fraction of MUA + MUA pairs than predicted by chance. However, what we find in the data is the opposite [Fig. 5(a)]. The proportion of MUA + MUA, SUA + SUA, and SUA + MUA pairs formed by the PRG procedure in its first iteration is similar to what one would obtain from random pairs.

We can also examine the final phase of the PRG procedure, i.e., the final grouping of neurons. In our case, at this stage coarse-grained variables represent sums of 64 raw variables. We calculate the fraction of MUAs to SUAs within each cluster [Fig. 5(b)]. As we can see, these fractions closely mirror those of the raw variables, indicating that MUA units are not inherently predisposed to being combined.

[1] K. Linkenkaer-Hansen, V. V. Nikouline, J. M. Palva, and R. J. Ilmoniemi, Long-range temporal correlations and scaling behavior in human brain oscillations, J. Neurosci. **21**, 1370 (2001).

[2] J. M. Beggs and D. Plenz, Neuronal avalanches in neocortical circuits, J. Neurosci. **23**, 11167 (2003).

[3] D. R. Chialvo, Emergent complex neural dynamics, Nat. Phys. **6**, 744 (2010).

[4] W. Shew and D. Plenz, The functional benefits of criticality in the cortex, Neuroscientist **19**, 88 (2013).

[5] J. M. Beggs, The criticality hypothesis: How local cortical networks might optimize information processing, Philos. Trans. R. Soc., A **366**, 329 (2008).

[6] M. A. Muñoz, Colloquium: Criticality and dynamical scaling in living systems, Rev. Mod. Phys. **90**, 031001 (2018).

[7] D. Plenz and E. Niebur (eds.), *Criticality in Neural Systems* (Wiley, Weinheim, 2014).

[8] N. Tomen, M. J. Herrmann, and U. Ernst, *The Functional Role of Critical Dynamics in Neural Systems* (Springer, Cham, Switzerland, 2019).

[9] L. de Arcangelis, C. Perrone-Capano, and H. J. Herrmann, Self-organized criticality model for brain plasticity, Phys. Rev. Lett. **96**, 028107 (2006).

[10] O. Kinouchi and M. Copelli, Optimal dynamical range of excitable networks at criticality, Nat. Phys. **2**, 348 (2006).

[11] A. Levina, J. M. Herrmann, and T. Geisel, Dynamical synapses causing self-organized criticality in neural networks, Nat. Phys. **3**, 857 (2007).

[12] A. Levina, J. M. Herrmann, and T. Geisel, Phase transitions towards criticality in a neural system with adaptive interactions, Phys. Rev. Lett. **102**, 118110 (2009).

[13] D. Fraiman, P. Balenzuela, J. Foss, and D. R. Chialvo, Ising-like dynamics in large-scale functional brain networks, Phys. Rev. E **79**, 061922 (2009).

[14] J. A. Bonachela and M. A. Muñoz, Self-organization without conservation: True or just apparent scale-invariance? J. Stat. Mech. (2009) P09009.

[15] J. A. Bonachela, S. de Franciscis, J. J. Torres, and M. A. Muñoz, Self-organization without conservation: Are neuronal avalanches generically critical? J. Stat. Mech. (2010) P02015.

[16] D. B. Larremore, W. L. Shew, and J. G. Restrepo, Predicting criticality and dynamic range in complex networks: Effects of topology, Phys. Rev. Lett. **106**, 058101 (2011).

[17] A. de Andrade Costa, M. Copelli, and O. Kinouchi, Can dynamical synapses produce true self-organized criticality? J. Stat. Mech. (2015) P06004.

[18] J. G. Ferreira Campos, A. de Andrade Costa, M. Copelli, and O. Kinouchi, Correlations induced by depressing synapses in critically self-organized networks with quenched dynamics, Phys. Rev. E **95**, 042303 (2017).

[19] S. Scarpetta, I. Apicella, L. Minati, and A. de Candia, Hysteresis, neural avalanches, and critical behavior near a first-order transition of a spiking neural network, Phys. Rev. E **97**, 062305 (2018).

[20] S. di Santo, P. Villegas, R. Burioni, and M. A. Muñoz, Landau–Ginzburg theory of cortex dynamics: Scale-free avalanches emerge at the edge of synchronization, Proc. Natl. Acad. Sci. USA **115**, E1356 (2018).

[21] O. Kinouchi, L. Brochini, A. A. Costa, J. G. F. Campos, and M. Copelli, Stochastic oscillations and dragon king avalanches in self-organized quasi-critical systems, Sci. Rep. **9**, 3874 (2019).

[22] O. Kinouchi, R. Pazzini, and M. Copelli, Mechanisms of self-organized quasicriticality in neuronal network models, Front. Phys. **8**, 583213 (2020).

[23] A. de Candia, A. Sarracino, I. Apicella, and L. de Arcangelis, Critical behaviour of the stochastic Wilson-Cowan model, PLoS Comput. Biol. **17**, e1008884 (2021).

[24] T. T. A. Carvalho, A. J. Fontenele, M. Girardi-Schappo, T. Feliciano, L. A. A. Aguiar, T. P. L. Silva, N. A. P. de Vasconcelos, P. V. Carelli, and M. Copelli, Subsampled directed-percolation models explain scaling relations experimentally observed in the brain, Front. Neural Circuits **14**, 576727 (2021).

[25] M. K. Nandi, A. Sarracino, H. J. Herrmann, and L. de Arcangelis, Scaling of avalanche shape and activity power spectrum in neuronal networks, Phys. Rev. E **106**, 024304 (2022).

[26] H. C. Piuvezam, B. Marin, M. Copelli, and M. A. Muñoz, Unconventional criticality, scaling breakdown, and diverse universality classes in the Wilson-Cowan model of neural dynamics, Phys. Rev. E **108**, 034110 (2023).

[27] J. M. Beggs and D. Plenz, Neuronal avalanches are diverse and precise activity patterns that are stable for many hours in cortical slice cultures, J. Neurosci. **24**, 5216 (2004).

[28] C. Haldeman and J. M. Beggs, Critical branching captures activity in living neural networks and maximizes the number of metastable states, Phys. Rev. Lett. **94**, 058101 (2005).

[29] C. V. Stewart and D. Plenz, Inverted-U profile of dopamine-NMDA-mediated spontaneous avalanche recurrence in superficial layers of rat prefrontal cortex, J. Neurosci. **26**, 8148 (2006).

[30] D. Plenz and T. C. Thiagarajan, The organizing principles of neuronal avalanches: Cell assemblies in the cortex? Trends Neurosci. **30**, 101 (2007).

[31] V. Pasquale, P. Massobrio, L. L. Bologna, M. Chiappalone, and S. Martinoia, Self-organization and neuronal avalanches in networks of dissociated cortical neurons, Neuroscience **153**, 1354 (2008).

[32] W. Shew, H. Yang, T. Petermann, R. Roy, and D. Plenz, Neuronal avalanches imply maximum dynamic range in cortical networks at criticality, J. Neurosci. **29**, 15595 (2009).

[33] T. Petermann, T. C. Thiagarajan, M. A. Lebedev, M. A. L. Nicolelis, D. R. Chialvo, and D. Plenz, Spontaneous cortical activity in awake monkeys composed of neuronal avalanches, Proc. Natl. Acad. Sci. USA **106**, 15921 (2009).

[34] T. L. Ribeiro, M. Copelli, F. Caixeta, H. Belchior, D. R. Chialvo, M. A. L. Nicolelis, and S. Ribeiro, Spike avalanches exhibit universal dynamics across the sleep-wake cycle, PLoS ONE **5**, e14129 (2010).

[35] F. Lombardi, H. J. Herrmann, C. Perrone-Capano, D. Plenz, and L. de Arcangelis, Balance between excitation and inhibition controls the temporal organization of neuronal avalanches, Phys. Rev. Lett. **108**, 228703 (2012).

[36] E. Tagliazucchi, P. Balenzuela, D. Fraiman, and D. R. Chialvo, Criticality in large-scale brain fMRI dynamics unveiled by a novel point process analysis, Front. Physiol. **3**, 15 (2012).

[37] H. Yang, W. L. Shew, R. Roy, and D. Plenz, Maximal variability of phase synchrony in cortical networks with neuronal avalanches, J. Neurosci. **32**, 1061 (2012).

[38] J. M. Palva, A. Zhigalov, J. Hirvonen, O. Korhonen, K. Linkenkaer-Hansen, and S. Palva, Neuronal long-range

temporal correlations and avalanche dynamics are correlated with behavioral scaling laws, Proc. Natl. Acad. Sci. USA **110**, 3585 (2013).

[39] O. Shriki, J. Alstott, F. Carver, T. Holroyd, R. N. Henson, M. L. Smith, R. Coppola, E. Bullmore, and D. Plenz, Neuronal avalanches in the resting MEG of the human brain, J. Neurosci. **33**, 7079 (2013).

[40] S. H. Gautam, T. T. Hoang, K. McClanahan, S. K. Grady, and W. L. Shew, Maximizing sensory dynamic range by tuning the cortical state to criticality, PLoS Comput. Biol. **11**, e1004576 (2015).

[41] W. L. Shew, W. P. Clawson, J. Pobst, Y. Karimipanah, N. C. Wright, and R. Wessel, Adaptation to sensory input tunes visual cortex to criticality, Nat. Phys. **11**, 659 (2015).

[42] A. Zhigalov, G. Arnulfo, L. Nobili, S. Palva, and J. M. Palva, Relationship of fast- and slow-timescale neuronal dynamics in human MEG and SEEG, J. Neurosci. **35**, 5385 (2015).

[43] A. J. Fontenele, N. A. P. de Vasconcelos, T. Feliciano, L. A. A. Aguiar, C. Soares-Cunha, B. Coimbra, L. Dalla Porta, S. Ribeiro, A. J. Rodrigues, N. Sousa, P. V. Carelli, and M. Copelli, Criticality between cortical states, Phys. Rev. Lett. **122**, 208101 (2019).

[44] N. Lotfi, A. J. Fontenele, T. Feliciano, L. A. A. Aguiar, N. A. P. de Vasconcelos, C. Soares-Cunha, B. Coimbra, A. J. Rodrigues, N. Sousa, M. Copelli, and P. V. Carelli, Signatures of brain criticality unveiled by maximum entropy analysis across cortical states, Phys. Rev. E **102**, 012408 (2020).

[45] N. Lotfi, T. Feliciano, L. A. A. Aguiar, T. P. L. Silva, T. T. A. Carvalho, O. A. Rosso, M. Copelli, F. S. Matias, and P. V. Carelli, Statistical complexity is maximized close to criticality in cortical dynamics, Phys. Rev. E **103**, 012415 (2021).

[46] E. Capek, T. L. Ribeiro, P. Kells, K. Srinivasan, S. R. Miller, E. Geist, M. Victor, A. Vakili, S. Pajevic, D. R. Chialvo *et al.*, Parabolic avalanche scaling in the synchronization of cortical cell assemblies, Nat. Commun. **14**, 2555 (2023).

[47] S. R. Miller, S. Yu, and D. Plenz, The scale-invariant, temporal profile of neuronal avalanches in relation to cortical γ-oscillations, Sci. Rep. **9**, 16403 (2019).

[48] N. Friedman, S. Ito, B. A. W. Brinkman, M. Shimono, R. E. L. DeVille, K. A. Dahmen, J. M. Beggs, and T. C. Butler, Universal critical dynamics in high resolution neuronal avalanche data, Phys. Rev. Lett. **108**, 208102 (2012).

[49] G. Chen, F. Scherr, and W. Maass, A data-based large-scale model for primary visual cortex enables brain-like robust and versatile visual processing, Sci. Adv. **8**, eabq7592 (2022).

[50] J. H. Kaas and C. Collins, The organization of sensory cortex, Curr. Opin. Neurobiol. **11**, 498 (2001).

[51] R. Yuste, From the neuron doctrine to neural networks, Nat. Rev. Neurosci. **16**, 487 (2015).

[52] A. Arieli, A. Sterkin, A. Grinvald, and A. Aertsen, Dynamics of ongoing activity: Explanation of the large variability in evoked cortical responses, Science **273**, 1868 (1996).

[53] M. Tsodyks, T. Kenet, A. Grinvald, and A. Arieli, Linking spontaneous activity of single cortical neurons and the underlying functional architecture, Science **286**, 1943 (1999).

[54] D. L. Ringach, Spontaneous and driven cortical activity: Implications for computation, Curr. Opin. Neurobiol. **19**, 439 (2009).

[55] K. D. Harris and A. Thiele, Cortical state and attention, Nat. Rev. Neurosci. **12**, 509 (2011).

[56] W. R. Softky and C. Koch, The highly irregular firing of cortical cells is inconsistent with temporal integration of random epsps, J. Neurosci. **13**, 334 (1993).

[57] G. R. Holt, W. R. Softky, C. Koch, and R. J. Douglas, Comparison of discharge variability in vitro and in vivo in cat visual cortex neurons, J. Neurophysiol. **75**, 1806 (1996).

[58] M. P. Nawrot, C. Boucsein, V. R. Molina, A. Riehle, A. Aertsen, and S. Rotter, Measurement of variability dynamics in cortical spike trains, J. Neurosci. Methods **169**, 374 (2008).

[59] A. Renart, J. de la Rocha, P. Bartho, L. Hollender, N. Parga, A. Reyes, and K. D. Harris, The asynchronous state in cortical circuits, Science **327**, 587 (2010).

[60] M. L. Schölvinck, A. B. Saleem, A. Benucci, K. D. Harris, and M. Carandini, Cortical state determines global variability and correlations in visual cortex, J. Neurosci. **35**, 170 (2015).

[61] E. A. Clement, A. Richard, M. Thwaites, J. Ailon, S. Peters, and C. T. Dickson, Cyclic and sleep-like spontaneous alternations of brain state under urethane anaesthesia, PLoS ONE **3**, e2004 (2008).

[62] M. Girardi-Schappo, L. Brochini, A. A. Costa, T. T. A. Carvalho, and O. Kinouchi, Synaptic balance due to homeostatically self-organized quasicritical dynamics, Phys. Rev. Res. **2**, 012042(R) (2020).

[63] L. Meshulam, J. L. Gauthier, C. D. Brody, D. W. Tank, and W. Bialek, Coarse graining, fixed points, and scaling in a large population of neurons, Phys. Rev. Lett. **123**, 178103 (2019).

[64] K. Wilson, Renormalization group and critical phenomena. I. renormalization group and the Kadanoff scaling picture, Phys. Rev. B **4**, 3174 (1971).

[65] N. A. P. de Vasconcelos, C. Soares-Cunha, A. J. Rodrigues, S. Ribeiro, and N. Sousa, Coupled variability in primary sensory areas and the hippocampus during spontaneous activity, Sci. Rep. **7**, 46077 (2017).

[66] G. Paxinos and K. Ashwell, *Atlas of the Developing Rat Nervous System* (Academic, San Diego, 2018).

[67] G. Nicoletti, S. Suweis, and A. Maritan, Scaling and criticality in a phenomenological renormalization group, Phys. Rev. Res. **2**, 023144 (2020).

[68] S. Bradde and W. Bialek, PCA meets RG, J. Stat. Phys. **167**, 462 (2017).

[69] A. Litwin-Kumar and B. Doiron, Slow dynamics and high variability in balanced cortical networks with clustered connections, Nat. Neurosci. **15**, 1498 (2012).

[70] An exception to this case could occur if the system had a Griffiths phase, with generic power-law scaling in a finite region of parameter space [84]. However, in this case, one would expect continuously varying exponents, which is not what we observe in the urethane data.

[71] See Supplemental Material at http://link.aps.org/supplemental/10.1103/PRXLife.2.023008 for an analysis of how the choice of bin duration affects scaling exponents, a definition of P(CV, Scaling) and results of state-dependent analysis for each animal.

[72] V. Priesemann, M. Wibral, M. Valderrama, R. Pröpper, M. Le Van Quyen, T. Geisel, J. Triesch, D. Nikolić, and M. H. J. Munk, Spike avalanches in vivo suggest a driven, slightly subcritical brain state, Front. Syst. Neurosci. **8**, 108 (2014).

[73] Z. Ma, G. G. Turrigiano, R. Wessel, and K. B. Hengen, Cortical circuit dynamics are homeostatically tuned to criticality in vivo, Neuron **104**, 655 (2019).

[74] S. A. Jones, J. H. Barfield, V. K. Norman, and W. L. Shew, Scale-free behavioral dynamics directly linked with scale-free cortical dynamics, Elife **12**, e79950 (2023).

[75] G. Morales, S. Di Santo, and M. Muñoz, Quasiuniversal scaling in mouse-brain neuronal activity stems from edge-of-instability critical dynamics, Proc. Natl. Acad. Sci. USA **120**, e2208998120 (2023).

[76] A. J. Fontenele, J. S. Sooter, V. K. Norman, S. H. Gautam, and W. L. Shew, Low-dimensional criticality embedded in high-dimensional awake brain dynamics, Sci. Adv. **10**, eadj9303 (2024).

[77] D. Dahmen, S. Grün, M. Diesmann, and M. Helias, Second type of criticality in the brain uncovers rich multiple-neuron dynamics, Proc. Natl. Acad. Sci. USA **116**, 13051 (2019).

[78] J. O'Byrne and K. Jerbi, How critical is brain criticality? Trends Neurosci. **45**, 820 (2022).

[79] M. C. Morrell, A. J. Sederberg, and I. Nemenman, Latent dynamical variables produce signatures of spatiotemporal criticality in large biological systems, Phys. Rev. Lett. **126**, 118302 (2021).

[80] O. Kinouchi and C. P. C. Prado, Robustness of scale invariance in models with self-organized criticality, Phys. Rev. E **59**, 4964 (1999).

[81] A. A. Costa, L. Brochini, and O. Kinouchi, Self-organized supercriticality and oscillations in networks of stochastic spiking neurons, Entropy **19**, 399 (2017).

[82] L. J. Fosque, R. V. Williams-García, J. M. Beggs, and G. Ortiz, Evidence for quasicritical brain dynamics, Phys. Rev. Lett. **126**, 098101 (2021).

[83] A. Ponce-Alvarez, M. L. Kringelbach, and G. Deco, Critical scaling of whole-brain resting-state dynamics, Commun. Biol. **6**, 627 (2023).

[84] P. Moretti and M. A. Muñoz, Griffiths phases and the stretching of criticality in brain networks, Nat. Commun. **4**, 2521 (2013).